# Hot-Electron Production and Wave Structure in a Helicon Plasma Source

A. W. Molvik, A. R. Ellingboe, and T. D. Rognlien
*Lawrence Livermore National Laboratory, Livermore, California 94551*
(Received 7 November 1996)

Energetic wave-trapped electrons of ~20 eV, moving at the 13.56 MHz helicon wave phase velocity, are directly measured with a 3 ns response-time retarding-potential analyzer. The rf axial wavelength is measured with $B$-dot probes scanned axially. Changes in the axial magnetic field or the rf power cause order of magnitude changes in the energetic electron current. The current correlates with either a transition from partially propagating to nearly pure standing waves or quantized jumps in the number of half wavelengths between the two azimuthal antenna straps. [S0031-9007(97)03548-5]

PACS numbers: 52.50.Dg, 52.40.Db, 52.70.Ds, 52.70.Nc

Pulses of argon line radiation have been reported [1] at the heating frequency in a helicon plasma source: the pulses originated in the near field of the antenna and propagated at the helicon wave phase velocity, consistent with trapping and accelerating pulses of electrons to 30 eV in the radio-frequency (rf) fields under the antenna. We report on strong variations in the current of energetic, wave-trapped electron pulses with changes in the magnitude of the axial magnetic field or rf power. The electrons are directly measured with a retarding-potential analyzer, having sufficient time response to resolve 15° of phase angle of the 13.56 MHz rf wave. We have previously shown that the energetic electrons are wave-trapped within a 75° FWHM phase angle each rf cycle [2]. This supports the picture that electrons "surf" on the helicon wave [1]; although, for our parameters, a given electron is expected to remain trapped for only a mean-free path of ~4 cm (limited by electron-neutral collisions) which is less than the helicon wavelength of ~20 cm. Orbit code calculations are used to assess this effect.

While Langmuir probes are a more common method of measuring the electron energy distribution function, the proper technique in rf fields continues to be controversial [3–5]. Retarding-potential gridded-energy analyzers (GEA) avoid these uncertainties; however, only electrons with axial energy exceeding the sheath potential drop can be detected. Sheath potential oscillations at the heating frequency are small. The primary diagnostic for this paper is a 1.9 cm diameter GEA [2,6] with grid voltages swept to measure electron and ion distribution functions. The distance between the last grounded entrance grid and the collector is 0.20 cm, providing 1 ns time response for 20 eV electrons, limited to 3 ns (corresponding to 15° of phase) by the 150 MHz analog bandwidth recorder. For 5 eV argon ions, the response time of 400 ns averages the ion distribution over 6 wave periods, so plasma potential measurements are not phase resolved. The GEA and other probes are downstream of the antenna region where hot electrons are produced, so should not perturb these data.

Helicon sources are attractive for plasma processing and a number of other applications because they provide high plasma density in low magnetic fields, with a high ionization efficiency, and a low, ~3 eV, electron temperature [7–9]. These features have motivated a number of groups to investigate helicons [10–17], much of which is summarized in a review paper [18].

The LLNL Helicon Source and diagnostics have been described [2], with data establishing that the plasma source operates in the helicon regime, with parameters appropriate for plasma processing. Several diagnostics are used for this paper in addition to the GEA: a movable $B$-dot probe array measures 3 orthogonal components ($B_r$, $B_\theta$, and $B_z$) at 6 radial positions from 0 to 7 cm [19], a 94 GHz interferometer measures electron line density at $z = 15$ cm, a movable Langmuir probe measures the plasma density, and a high impedance probe [20] measures the rf floating potential, $V_f$. The axially movable diagnostics are inserted from $z = 85$ cm. A capacitance manometer at the end of a 60 cm long, 1.3 cm diameter Pyrex tube [21], inserted to $z = 30$ cm from $z = 0$ cm, measures the argon pressure on axis to be ~6 mTorr without plasma, decreasing to 4.5 mTorr with plasma at our operating conditions. The dc magnetic field is nearly constant between $z = 8$ and 25 cm, which includes the open area of an $m = 1$ Nagoya Type III antenna that has 2.5 cm wide azimuthal straps centered at $z = 11.2$ and 26.8 cm.

The rf power is provided by a 3 kW, 13.56 MHz amplifier, gated on for times ranging between 80 ms and 8 s, every several minutes. The plasma density rises within 100 $\mu$s, reaching steady state after 50 ms. The energetic electron current remains near zero for the first 1.5 ms, approaches its steady-state value by 3 ms, and has been measured at this value out to 400 ms where we stop taking GEA data. All GEA data shown in this paper are taken at 80 ms. The $B$-dot data were taken by scanning the probe axially during a 5 s plasma shot.

To optimize performance, we vary the axial magnetic field ($B_0 \equiv$ peak value of $B$) from shot to shot. Simultaneously, we measure the energetic electron current and energy distribution at $z = 30$ cm, near the peak of the axial profile of energetic electrons. The GEA is located off axis at a radius of 2.5 cm, at $\theta$ of 0° or 180° on the horizontal midplane. The GEA electron repeller grid voltage $V_g$ is swept on each shot. The energy distributions are

  

similar to that published previously [2]. Varying $B_0$ is expected to change the wave phase velocity, $v_{ph}$, according to the helicon dispersion relation [18]

$$v_{ph} = \frac{\omega}{k} = \left(\frac{\beta}{a}\right)\left(\frac{\omega_{ce}c^2}{\omega_{pe}^2}\right) = \frac{1.9 \times 10^{19}}{a}\frac{B_0}{n_0}, \quad (1)$$

where $\beta \approx 3.8$ for the first radial eigenmode, $B_0$ is in G, the electron density $n_0$ is in $cm^{-3}$, and the plasma radius $a$ is in cm. Electron energies below the difference between the plasma potential $V_p$ and the floating potential $V_f$ are repelled by the plasma sheath potential $V_s$ and cannot enter the analyzer. For unmagnetized, Maxwellian, argon plasmas, $qV_s = q(V_p - V_f) = 5.6T_e \sim 17$ eV (for $T_e = 3$ eV), similar to the measured $V_s = 15$ V. The entrance grids are grounded to the end wall, placing both at an averaged $V_f \equiv 0$, so $V_s \approx V_p$. For a Maxwellian with thermal energy $E_t$, the electron current measured by the GEA would vary as $\exp[-q(V_g + V_s)/E_t]$ for negative grid voltage $V_g$. The results in Fig. 1 show more structure than expected. At $\theta = 180°$, a change of $B_0$ from 90 to 100 G reduces the energetic electron current from 25 $mA/cm^2$ to near zero as shown in Fig. 1(a); and at $\theta = 0°$, a reduction from 21 to 6 $mA/cm^2$ occurs between 63 and 70 G in Fig. 1(b). The energetic electron current is reduced for $B_0 < 50$ G at both $\theta = 0°$ and 180°. The energetic electron current was previously observed to switch phase 180° across the midplane [1]; however, the differences here between $\theta = 0°$ and 180° indicate azimuthal asymmetries.

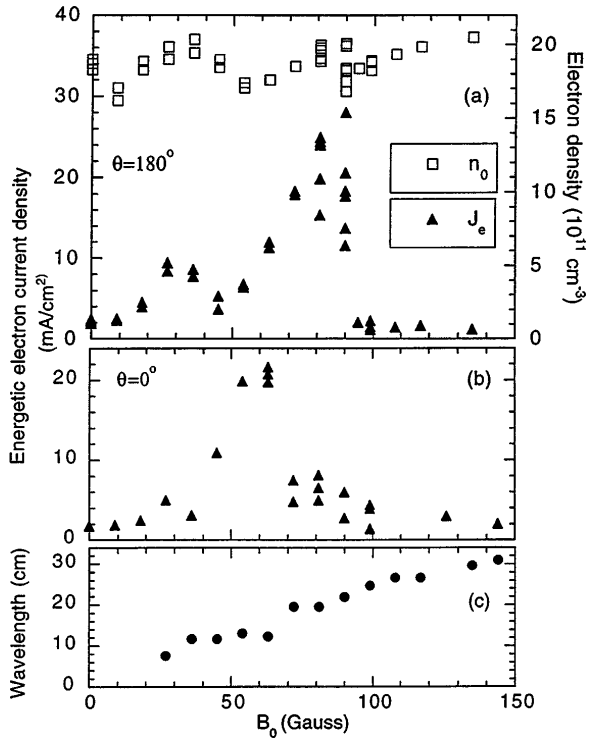


FIG. 1. As a function of magnetic field $B_0$ (a) line-averaged density at $z = 15$ cm and energetic electron current density incident on energy analyzer, at radius of 2.5 cm and $z = 30$ cm, and on horizontal midplane at $\theta = 180°$; (b) the analyzer at $\theta = 0°$; (c) rf wavelength from $B$-dot probe at a radius of 3 cm measured between $z = 20$ and 30 cm.

The peak in the energetic electron current density occurs between $B_0 = 60$–$90$ G where the helicon phase velocity corresponds to electrons at ~20 eV. Measurements of the plasma potential (15 ± 5 V) are obtained from the minimum ion energy. The energetic electron energy distribution is approximately uniform over a 10 eV range above $qV_s$, i.e., from 15 to 25 eV [2]. These GEA data verified that the hot-electron velocity was approximately equal to the helicon phase velocity for these parameters.

We also obtain dramatic variations in energetic electron current by fixing $B_0$ at 63 G and varying the rf power from shot to shot, as shown in Fig. 2. Here the electron energy analyzer is at 2.5 cm radius and $\theta = 0°$, and a Langmuir probe is at 2.5 cm radius and $\theta = 15°$ above the analyzer, both at $z = 30$ cm. The source operates in any of the three modes: $E$, $H$, or $W$, identified by Ellingboe [19]. The modes are separated by jumps in rf power and density, and for fixed $B_0$ are selected by the rf power. The energetic electron current is nonzero only in the $W$ mode, where helicon waves propagate with finite $B_z$ dot [19]. The second jump in electron current density, to 16 $mA/cm^2$, has not been correlated with changes in other parameters. Following Eq. (1), we can obtain helicon (i.e., $W$ mode) operation at the desired $v_{ph}$ either by varying $B_0$ or by varying $n_0$ through changing the rf power.

The difference between the density at $z = 15$ cm, Fig. 1(a), and that at $z = 30$ cm, Fig. 2, is largely due to the axial plasma density profile. The profile was measured at an argon fill pressure of 14 mTorr to peak near $z = 15$ cm (the interferometer location), and to decrease to 28% of peak at $z = 30$ cm, but was not measured at our standard 6 mTorr. The density in Fig. 2 is also a lower limit because the probe bias of −30 V is apparently insufficient to repel all energetic electrons, causing the probe current to vary inversely with the energetic electron current density in some runs. From the density and magnetic field profiles, we compute the rf wavelength using Eq. (1). The wavelength varies from a minimum of 10 cm at $z = 15$ cm, to ~20 cm at $z = 25$ cm, and

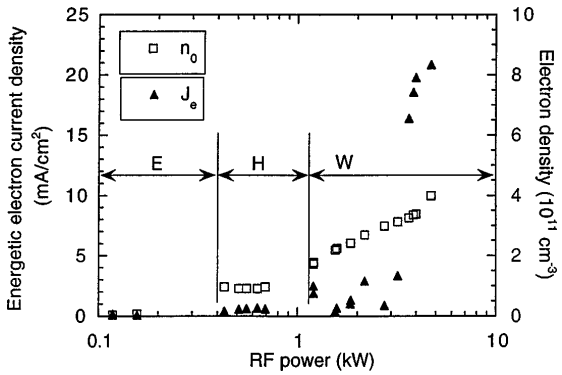


FIG. 2. Magnitude of energetic electron current density, and density from ion saturation current, plotted versus rf power. The $E$, $H$, $W$-mode notation is from Ref. [19].

a maximum of 30 to 40 cm at $z \geq 30$ cm. The $B_z$-dot data are consistent with this from 20 to 30 cm as shown in Fig. 1(c), and near $z = 15$ cm, but beyond 30 cm show the wavelength decreasing. The rf wave amplitude decreases more rapidly than the flux tube expansion would require, because the $k_z$ spectrum launched by the antenna no longer matches the propagation requirement of Eq. (1).

We investigate the possible perturbation of the GEA data by oscillations in $V_p$, i.e., sheath potential. First, we use a $V_f$ probe, which achieves response times of 5 ns with a 12 k$\Omega$ ($\gg R_{\text{sheath}} \sim 1$ k$\Omega$) resistor near the tip [20]. The probe tip, 0.5 cm long by 0.05 cm diameter, is aligned parallel to the magnetic field, decreasing the effective probe area for hot electrons. We determine that energetic electron pulses occur during positive spikes of $V_f$, every rf cycle. This shows that the electrons are not electrostatically expelled from a "Maxwellian" tail, which would occur during the negative half cycle of $V_f$. Second, if $V_p$ oscillations have sufficient amplitude, the electron energy distribution will vary with phase angle. We have found the electron energy distribution to be independent of phase angle when examined in 5–10° units over the 75° FWHM, and to look very much like Fig. 4 of Ref. [2]. This indicates that plasma potential oscillations are small ($\leq$1–2 V over 75° compared with the 10 eV width of the hot-electron distribution) which is consistent with axial electric fields as large as 0.2–0.5 V/cm for wavelengths of 20 cm. These results indicate that the GEA data is not significantly perturbed by an oscillating plasma potential.

To gain insight into the causes of the variations in energetic electron current, we measure the rf $B$-dot fields as a function of radial and axial positions at the same parameter ranges as in Figs. 1 and 2. The normalized axial profile of $B_0$ is shown in Fig. 3(a). Contours of $B_z$-dot magnitude at 3 values of $B_0$: 117, 72, and 36 G selected from Fig. 1, are plotted in Figs. 3(b)–3(d), respectively. The axial wavelength, measured between about $z = 20$ and 30 cm, remains nearly constant before jumping to a new value as shown in Fig. 1(c), rather than varying linearly with $B_0$ as inferred from Eq. (1). This is consistent with the antenna length fixing the wavelength until the optimum helicon wavelength, Eq. (1), shifts enough for the finite width $k_z$ spectrum of the antenna to launch more power into the new than into the old wavelength. The data at a radius of 3 cm are plotted vs $z$ at 8 different times in the rf cycle in Figs. 3(e)–3(g) for the same three magnetic fields. Both sets of plots show a jump in the number of half wavelengths between 72 and 36 G where a change in current is observed in Fig. 1. Comparing Figs. 3(b) and 3(e), 3(c) and 3(f), and 3(d) and 3(g) where each peak corresponds to 180° of phase change, the wavelengths are ~27, 20, and 12 cm, respectively, yielding phase velocities corresponding to resonant electron energies of 36, 20, and 7 eV. In Figs. 3(f) and 3(g), nearly pure standing waves are seen to be formed under the antenna, becoming propagating waves to the right of 25–28 cm. But in Fig. 3(e), the waves under the antenna are partially

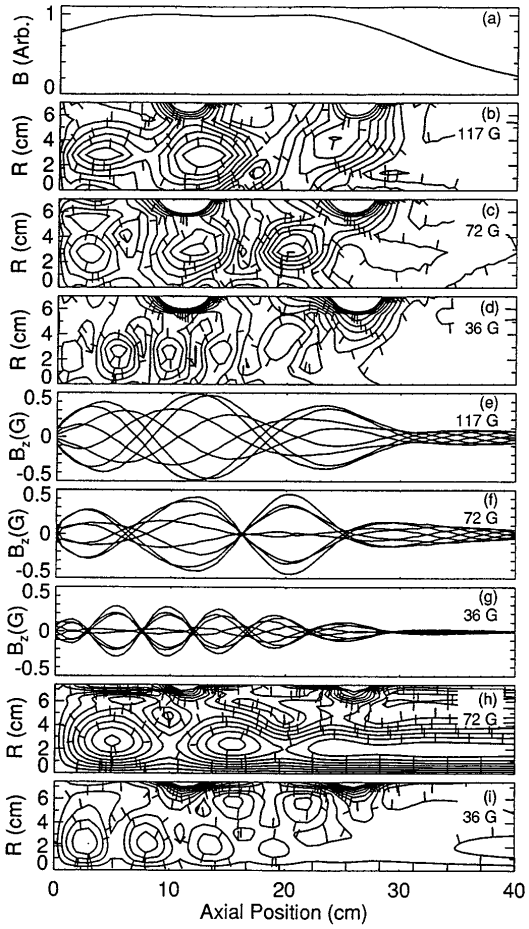


FIG. 3. (a) Magnetic field flares beyond $z = 25$ cm. (b), (c), (d) Contour plot of $B_z$-dot data at $\theta = 180°$ for $B_0$ under the antenna of 117, 72, and 36 G, respectively. Contours plotted in 0.05 G intervals, 0.05 to 0.5 G; "tic" marks point downhill. Type III azimuthal antenna straps produce large edge fields at $z = 11$ and 26 cm. (e), (f), (g) Magnitude of $B_z$ for 8 phase angles at radius of 3 cm and $B_0$ of 117, 72, and 36 G, respectively. (h), (i) Contours of $B_z$ computed by ANTENA code [22] for $B_0$ of 72 and 36 G, respectively.

propagating towards $z = 0$, thus accelerating electrons preferentially away from the detector.

In a 3 eV Maxwellian distribution, the fraction of electrons within $\pm 2$ eV of resonant energies of 7, 20, and 36 eV are 0.14, $1.9 \times 10^{-3}$, and $9 \times 10^{-6}$. For $n_0 = 1 \times 10^{12}$ cm$^{-3}$, this yields current densities of 3500, 80, and 0.5 mA/cm$^2$, respectively. From the absence of a hot electron signal near the above values, except at certain parameters as shown in Figs. 1 and 2, we infer that the tail of the electron energy distribution is truncated below Maxwellian values.

The mode patterns of the rf magnetic field are consistent with our calculations from the ANTENA code [22]. The plasma and magnetic field are assumed uniform in $z$, and the plasma density varies radially as $1 \times 10^{12}[1 - (r/10.5)^2]$. This density profile is guided by ion-saturation probe measurements. The full 3D structure of the Type III antenna is included, except for the radial leads. The electron collision frequency is taken as $1 \times 10^7$ s$^{-1}$ arising

from both neutral and Coulomb collisions near thermal energy. The results, shown in Figs. 3(h) and 3(i) for $B_0 = 72$ and 36 G, compare quite well with measured contours of Figs. 3(c) and 3(d), showing axial eigenmodes that vary with magnetic field with no anomalous effects required. The antenna current is estimated to be 15 A [2], compared to the 10 A value used in the ANTENA runs.

To model the electron heating, we use an electron orbit code that follows an ensemble of electrons in a prescribed rf axial electric field, $E_z$, having a standing wave pattern as found in the experiment and from ANTENA. The initial electron distribution is Maxwellian at 3 eV. These calculations are similar to those in Ref. [1], except that we also include the effect of neutral and Coulomb collisions. At a pressure of 5 mTorr, a strong enhancement of electrons to 20–25 eV is found for a wave phase velocity corresponding to 15 eV for $E_z \geq 0.5$ V/cm. The production of hot electrons with positive velocities is modulated at the wave frequency, as observed in the experiment. If the phase velocity is increased to correspond to an energy of 30 eV, the number of heated electrons becomes much smaller. At higher pressures, higher $E_z$ fields are necessary to overcome collisional scattering out of the wave. The $E_z = 0.5$ V/cm fields are a factor of 2–10 larger than computed by ANTENA with inputs appropriate to the experiment, an unexplained discrepancy. But, as noted, GEA data are consistent with $E_z$ as large as 0.2–0.5 V/cm.

A set of criteria for the generation and detection of energetic electrons can be formulated, based on our experimental measurements and models: First, models of energetic electron heating by helicon waves [1,2] show that standing waves provide transit-time heating of electrons by several eV, high enough for the electrons to be trapped and accelerated further when injected into accelerating traveling waves. All our data, including that presented here, are consistent with needing both standing and traveling waves. Second, only in $W$ mode do traveling waves exist that can trap and accelerate electrons in the core of the plasma column [19], so this mode is necessary for obtaining energetic electrons. Third, the rf-phase velocity must be matched to the electron energy distribution function. Fourth, electron energies below the sheath potential $V_s$ cannot enter the analyzer. Fifth, at higher pressure, neutral collisions scatter energetic electrons out of the wave. Effects three and four account for the peak of 20 eV electrons at 60–90 G in Fig. 1. This peak may be a lower limit, because portions of the tail pulled out of a truncated distribution may lie below the $V_s \sim 15$ eV detection limit. Thermal ionization that would be responsible for 85% of the ionization with a Maxwellian distribution will be reduced by a truncated distribution, relative to hot-electron ionization.

In conclusion, peak energetic electron current densities are measured when standing waves under the antenna couple to traveling helicon waves that have phase velocities corresponding to electron energies near 20 eV, high enough in energy to penetrate the sheath at the analyzer and low enough to have a significant number of electrons. Matching the phase velocity and achieving wave-mode operation can be realized with a magnetic field in the 50–100 G range and sufficient rf power to achieve densities the order of $10^{12}$ cm$^{-3}$. In this way, the magnetic field $B_0$ and the rf power provide convenient variables to control the current of energetic electrons [23].

The support and encouragement of J. N. Bardsley, E. B. Hooper, and the LLNL LDRD Program are gratefully acknowledged. H. S. McLean programmed the data acquisition system, R. A. Rego designed and built the GEA, and R. A. Breun suggested the capacitance manometer pressure measurements. This work was performed under the auspices of the U.S. Department of Energy by LLNL under Contract No. W-7405-ENG-48.

[1] A. R. Ellingboe, R. W. Boswell, J. P. Booth, and N. Sadeghi, Phys. Plasmas **2**, 1807 (1995).
[2] A. W. Molvik *et al.*, J. Vac. Sci. Technol. A **14**, 984 (1996).
[3] N. Hershkowitz, in *Plasma Diagnostics*, edited by O. Auciello and D. L. Flamm (Academic Press, San Diego, CA, 1989), Vol. 1, p. 162.
[4] I. D. Sudit and F. F. Chen, Plasma Sources Sci. Technol. **3**, 162 (1994).
[5] V. A. Godyak, R. B. Piejak, and B. M. Alexandrovich, Plasma Sources Sci. Technol. **4**, 332 (1995); J. Appl. Phys. **73**, 3657 (1993).
[6] A. W. Molvik, Rev. Sci. Instrum. **52**, 704 (1981).
[7] R. W. Boswell, Phys. Lett. **33A**, 457 (1970).
[8] R. W. Boswell, Plasma Phys. Controlled Fusion **26**, 1147 (1984).
[9] A. W. Degeling, C. O. Jung, R. W. Boswell, and A. R. Ellingboe, Phys. Plasmas **3**, 2788 (1996).
[10] P. K. Loewenhardt *et al.*, Phys. Rev. Lett. **67**, 2792 (1991).
[11] A. Komori *et al.*, Phys. Fluids B **3**, 893 (1991).
[12] F. F. Chen, J. Vac. Sci. Technol. A **10**, 1389 (1992).
[13] V. P. Katyukha *et al.*, Rev. Sci. Instrum. **65**, 1368 (1994).
[14] P. K. Loewenhardt, B. D. Blackwell, and S. M. Hamberger, Phys. Plasmas **1**, 875 (1994).
[15] R. T. S. Chen *et al.*, Plasma Sources Sci. Technol. **4**, 337 (1995).
[16] K. Nakamura, K. Suzuki, and H. Sugai, Jpn. J. Appl. Phys. **34**, 2152 (1995).
[17] H. Takeno *et al.*, Nucl. Fusion **35**, 75 (1995).
[18] F. F. Chen, in *High Density Plasma Sources*, edited by Oleg A. Popov (Noyes Publications, Park Ridge, NJ, 1995), Chap. 1.
[19] A. R. Ellingboe and R. W. Boswell, Phys. Plasmas **3**, 2797 (1996).
[20] J. C. Sprott, Rev. Sci. Instrum. **37**, 897 (1966).
[21] J. Gilland, R. Breun, and N. Hershkowitz, Bull. Am. Phys. Soc. **40**, 1580 (1995).
[22] See National Information Service Document No. DE85004960 (B. McVey, Plasma Fusion Center, MIT, Report No. PFC/RR-84-12). Copies may be ordered from the National Technical Information Service, Springfield, VA 22161.
[23] Patent applied for.